

A Unified [CII] Morpho-Kinematic Corpus for 31 Star-Forming Galaxies at $z = 4.26$ – 5.68 : The High- z Kinematic Corpus Z1

DAVID C. FLYNN¹

¹*EPS Research, Laurel, MD, USA; ORCID: 0000-0002-2768-6650*

ABSTRACT

We present the High- z Kinematic Corpus Z1, a structured machine-readable dataset of ALMA [CII] 158 μm morpho-kinematic data for 31 star-forming main-sequence galaxies at $z = 4.26$ – 5.68 drawn from the ALPINE survey (Jones et al. 2021; Le Fèvre et al. 2020). The corpus is the fourth and final entry in the EPS Research RAG Astrophysics Corpus Series, extending coverage from Milky Way globular clusters and local HI rotation curves (Flynn 2026a,b,c) to the epoch approaching cosmic reionization. Eight confirmed rotators carry quality tier 1 per-ring rotation curves from 3DBarolo tilted-ring fits (Di Teodoro & Fraternali 2015), with 2–3 rings per galaxy, V_{rot} and σ per ring, and dynamical mass estimates; the remaining 23 galaxies carry morpho-kinematic classification only (quality tier 2). All entries include stellar mass (Faisst et al. 2020), star formation rate, Wisnioski et al. (2015) disk criteria, and geometric parameters. The corpus is distributed as a single structured JSON file with nested per-ring kinematic data, a flat CSV for catalog-level filtering, a RAG-ready JSONL archive (one galaxy per line), and a per-galaxy ZIP archive. Three worked Jupyter notebook examples demonstrate single-galaxy [CII] rotation curve analysis, corpus-level population statistics, and cross-corpus application of the Flynn & Cannaliato (2025) omega kinematic correction. Applying the omega formula to all 8 tier-1 rotators yields negative values (median $-13.05 \text{ rad Gyr}^{-1}$), contrasting with positive values at $z = 0$ ($+7.06 \text{ rad Gyr}^{-1}$ for SPARC spirals; $+9.94 \text{ rad Gyr}^{-1}$ for local dwarfs), consistent with the known evolution from centrally concentrated high- z systems to extended rotating disks. The corpus is publicly available at Zenodo (DOI: [10.5281/zenodo.20369285](https://doi.org/10.5281/zenodo.20369285)) under CC BY 4.0.

Keywords: high-redshift galaxies — galaxy kinematics — ALPINE survey — ALMA — [CII] 158 μm — rotation curves — RAG — LLM — data release — omega kinematic correction

1. INTRODUCTION

The kinematic properties of galaxies at $z \sim 4$ – 6 encode critical information about the assembly of rotating disk structures and the distribution of baryonic and dark matter in the early universe. At these redshifts, ALMA observations of the [CII] 158 μm fine-structure line provide the most reliable tracer of cold gas morphology and kinematics (Le Fèvre et al. 2020; Béthermin et al. 2020). The ALPINE survey (ALMA Large Program to INvestigate [CII] at Early Times) observed 118 main-sequence star-forming galaxies at $z = 4.4$ – 5.9 (Le Fèvre et al. 2020), of which Jones et al. (2021) published 3DBarolo tilted-ring kinematic models for a subset of confirmed ro-

tators and morpho-kinematic classifications for the full sample.

Despite the scientific importance of these data, no unified machine-readable corpus currently exists that combines the ALPINE kinematic catalog, per-ring rotation curve data, Wisnioski et al. (2015) disk criteria, stellar masses, and geometric parameters in a single self-describing schema. This data-fragmentation problem is particularly acute for computational workflows—including LLM-based retrieval-augmented generation (RAG) pipelines—that require structured, consistently typed input data.

This paper presents the High- z Kinematic Corpus Z1, a structured JSON dataset containing morpho-kinematic data for 31 ALPINE galaxies at $z = 4.26$ – 5.68 . The corpus is the fourth entry in the EPS Research RAG Astrophysics Corpus Series:

1. Unified HI Rotation Curve Corpus v7.0 (Flynn 2026a): 438 galaxies, $z = 0$, HI 21 cm
2. Dwarf/Irregular HI Rotation Curve Corpus v1.0 (Flynn 2026b): 129 galaxies, $z = 0$, HI 21 cm
3. Milky Way Globular Cluster Corpus v1.3.1 (Flynn 2026c): 174 clusters, multi-survey
4. **High- z Kinematic Corpus Z1 (this work)**: 31 galaxies, $z = 4.3\text{--}5.7$, [C II] 158 μm

Together these four corpora form a unified RAG knowledge base spanning Milky Way stellar clusters, local spiral and dwarf galaxies, and the epoch approaching cosmic reionization. We describe the corpus architecture (Section 2), the schema and quality tier system (Section 3), the ingestion and verification procedures (Section 4), three usage examples (Section 5), the LLM/RAG application (Section 6), known limitations (Section 7), and data availability (Section 8).

2. SOURCE DATA AND SURVEY COVERAGE

2.1. ALPINE Survey

The ALMA Large Program to INvestigate [C II] at Early Times (ALPINE; Le Fèvre et al. 2020; Béthermin et al. 2020) observed 118 main-sequence star-forming galaxies at $z = 4.4\text{--}5.9$ with ALMA in the [C II] 158 μm line (ALMA project 2017.1.00428.L). The survey was designed to characterize the cold gas content, morphology, and kinematics of typical star-forming galaxies during the epoch of peak cosmic star formation. The synthesized beam is approximately 1 arcsec FWHM, corresponding to $\sim 6\text{--}7$ kpc at $z \sim 5$, setting the practical spatial resolution floor for kinematic analysis.

2.2. Jones et al. (2021) Kinematic Catalog

Jones et al. (2021) applied the 3DBarolo tilted-ring fitter (Di Teodoro & Fraternali 2015) to a subset of ALPINE galaxies with sufficient [C II] signal-to-noise for kinematic modeling, publishing per-ring rotation velocities, velocity dispersions, and dynamical masses in their Table C1. Morpho-kinematic classifications (ROT, MER, DIS, UNC) are provided for the full sample in their Table 1, supplemented by the five Wisnioski et al. (2015) disk criteria (Wisnioski et al. 2015). This corpus ingests both tables as the primary kinematic source.

2.3. Ancillary Data

Stellar masses and star formation rates are drawn from the ALPINE multi-wavelength photometry catalog (Faisst et al. 2020), which provides SED-fitted M_* and SFR for all ALPINE targets. The ALPINE Data

Table 1. Corpus coverage summary.

Property	Value
Total galaxies	31
Redshift range	$z = 4.26\text{--}5.68$
Maximum redshift	$z = 5.6773$ (DC773957)
Survey	ALPINE
Telescope	ALMA
Tracer	[C II] 158 μm
Confirmed rotators (ROT)	8
Mergers (MER)	5
Dispersion-dominated (DIS)	3
Uncertain (UNC)	15
Quality tier 1	8
Quality tier 2	23

Release 1 (Béthermin et al. 2020) provides the [C II] flux catalog and morphological parameters.

Table 1 summarizes the corpus coverage.

3. CORPUS ARCHITECTURE AND SCHEMA

3.1. File Formats

The corpus is distributed in four complementary formats. The master file `high_z_kinematic_corpus.Z1.json` is a single JSON document containing all 31 galaxy entries within a unified schema, together with a top-level metadata block. The flat table `high_z_kinematic_corpus.Z1.flat.csv` provides one row per galaxy (31 rows) with summary statistics for sample selection and filtering. The JSONL file `high_z_kinematic_corpus.Z1.jsonl` contains one self-describing JSON object per line, optimized for LLM/RAG ingestion. The per-galaxy archive `high_z_kinematic_corpus.Z1_by_galaxy.zip` contains 31 individual JSON files, each self-contained with full corpus metadata and the complete rotation curve array.

3.2. Quality Tier System

A two-tier quality annotation is applied at the galaxy level. Tier 1 (8 confirmed rotators) denotes galaxies with per-ring V_{rot} , σ , and M_{dyn} from the Jones et al. (2021) 3DBarolo fits (their Table C1). Tier 2 (23 galaxies) denotes morpho-kinematic classification only, with no reliable rotation curve. The tier system enables downstream analyses to filter by data quality without inspecting individual galaxies.

Tier-1 qualification note: Although all 8 tier-1 entries carry per-ring fits from a peer-reviewed source,

Table 2. Per-galaxy schema summary.

Field	Type	Description
<code>galaxy</code>	str	Source name
<code>redshift</code>	float	Spectroscopic redshift
<code>class_jones2021</code>	str	ROT MER DIS UNC
<code>is_rotator</code>	bool	Boolean flag
<code>w15_criteria</code>	dict	Five W15 disk criteria
<code>inc_kin_deg</code>	float	Kinematic inclination
<code>pa_kin_deg</code>	float	Kinematic PA (deg)
<code>vrot_max_kms</code>	float	Peak rotation velocity
<code>sigma_mean_kms</code>	float	Mean velocity dispersion
<code>v_over_sigma</code>	float	Kinematic state indicator
<code>log_dyn_msun</code>	float	log ₁₀ dynamical mass
<code>log_mstar_msun</code>	float	log ₁₀ stellar mass
<code>sfr_msun_yr</code>	float	Star formation rate
<code>quality_tier</code>	int	1 (per-ring) 2 (class only)
<code>beam_smeared</code>	bool	True (all ALPINE)
<code>data</code>	list	Per-ring RC (tier 1 only)

NOTE—Per-ring `data` entries contain `R_kpc`, `Vrot_kms`, `e.Vrot_kms`, `sigma_kms`, `e.sigma_kms`, `Mdyn_msun`, and `v_over_sigma`. Tier-2 galaxies have an empty `data` array and null kinematic fields.

the astrophysical quality is limited by ALMA resolution (~ 1 arcsec beam, $\sim 6\text{--}7$ kpc at $z \sim 5$) and ring counts of 2–3 per galaxy. These are the best currently available spatially resolved [C II] rotation curves at $z \sim 4\text{--}6$, but are marginal by the standards of local HI surveys. Users applying quantitative kinematic analyses should treat tier-1 Z1 entries with commensurate caution.

3.3. Per-Galaxy Schema

Table 2 summarizes the per-galaxy fields available in the corpus.

3.4. Omega Correction Compatibility

The corpus schema is designed to support the Flynn & Cannaliato (2025) omega kinematic correction:

$$\omega = \left(\frac{V_2}{R_2} - \frac{V_1}{R_1} \right) \left(\frac{R_1}{R_2} \right)^{3/2} \quad [\text{rad Gyr}^{-1}] \quad (1)$$

where (R_1, V_1) and (R_2, V_2) are the innermost and outermost fitted ring boundary points. For tier-1 galaxies, `data[0]` provides $(R_1, V_{\text{rot},1})$ and `data[-1]` provides $(R_2, V_{\text{rot},2})$.

4. INGESTION AND VERIFICATION

4.1. ALPINE Data Ingestion

Kinematic parameters were ingested from Jones et al. (2021) Tables 1 and C1. Per-ring rotation velocities, velocity dispersions, dynamical masses, inclinations, and position angles for the 8 confirmed rotators were digitized from Table C1. Morpho-kinematic classifications, Wisnioski et al. (2015) criteria, and integrated kinematic parameters were ingested from Table 1. Stellar masses and SFRs were cross-matched from Faisst et al. (2020). Spectroscopic redshifts were drawn from the ALPINE catalog (B  thermin et al. 2020).

The ingestion pipeline (`alpine_ingest.py`) performs five steps: (1) galaxy-by-galaxy data ingestion from primary tables; (2) schema validation against the Z1 schema; (3) export to JSON, JSONL, CSV, and per-galaxy ZIP formats; (4) RAG example generation; and (5) README generation. All steps are fully scripted and reproducible from the deposited source files.

4.2. Schema Validation

A dedicated schema validator (`schema_validator_hz.py`) checks each galaxy entry for required field presence and type correctness, controlled vocabulary compliance (ROT|MER|DIS|UNC), Wisnioski criterion internal consistency (boolean flags vs. `n_passed` count), boolean flag consistency with `class_jones2021`, per-ring data monotonicity, and tier-1/tier-2 data completeness rules. All 31 galaxies pass validation with zero errors in standard mode; strict mode raises expected warnings for null kinematic fields in tier-2 galaxies, which carry no per-ring data by design.

4.3. Known Data Anomalies

Three data anomalies inherited from the primary source are documented in the corpus `known_issues` field:

CG32 and DC396844: $\log M_{\text{dyn}} < \log M_*$ by 0.16 and 0.35 dex respectively. Dynamical mass below stellar mass is physically implausible and likely reflects inclination uncertainty (DC396844 $e_{\text{inc}} = 31^\circ$) compounded by the 2-ring boundary constraint. Values are reported as published in Jones et al. (2021) Table C1.

HZ9 outer-ring dispersion: The outermost ring of HZ9 has $\sigma = 4.82 \text{ km s}^{-1}$, anomalously low relative to the inner rings ($\sigma \sim 71\text{--}75 \text{ km s}^{-1}$), producing $V/\sigma = 36.6$ at the outer boundary. This likely reflects a 3DBarolo fit artifact at the beam resolution limit.

DC519281 redshift uncertainty: $e_z = 0.02$, approximately $40\times$ larger than the typical uncertainty (~ 0.0005) in the sample.

5. USAGE EXAMPLES

The following three examples demonstrate the corpus utility for common high- z kinematic analyses. Each example is provided as a self-contained Jupyter notebook (deposited alongside the corpus) loading data directly from the JSON with no external preprocessing. All code uses Python 3 with only `numpy` and `matplotlib`. Output figures are deposited as supplementary material.

5.1. Example 1: [CII] Rotation Curve of a Confirmed Rotator

Figure 1 shows J0817, the highest-velocity confirmed rotator in the corpus ($V_{\text{rot,max}} = 252 \text{ km s}^{-1}$ at $z = 4.26$), with three panels extracted directly from the corpus JSON: V_{rot} with error bars (top), velocity dispersion profile (bottom left), and V/σ per ring (bottom right). The metadata annotation (inclination, PA, $\log M_{\text{dyn}}$, W15 criteria) is extracted directly from the JSON. The point for this data descriptor is that all three panels come from a single JSON load in under 15 lines of Python.

J0817 rotation curve from corpus JSON.

```
import json, numpy as np, matplotlib.pyplot as plt
with open('high_z_kinematic_corpus_Z1.json') as f:
    corpus = json.load(f)
g = next(g for g in corpus['galaxies']
         if g['galaxy'] == 'J0817')
d = g['data']
R = np.array([p['R_kpc'] for p in d])
Vrot = np.array([p['Vrot_kms'] for p in d])
eVrot = np.array([p['e_Vrot_kms'] for p in d])
sigma = np.array([p['sigma_kms'] for p in d])
vos = np.array([p['v_over_sigma'] for p in d])
plt.errorbar(R, Vrot, yerr=eVrot, fmt='o-')
```

Table 3 lists all 8 tier-1 rotators with outermost ring properties.

5.2. Example 2: Corpus-Level Population Statistics

Figure 2 provides the corpus population overview loaded from the flat CSV. Panel (a) shows the morphokinematic class fractions (ROT: 8, MER: 5, DIS: 3, UNC: 15). Panel (b) shows the redshift distribution by class as a stacked histogram, with the $z = 5$ boundary marked; 9 of 31 galaxies lie at $z > 5$, with 4 UNC, 3 ROT, 1 DIS, and 1 MER in this subsample. Panel (c) shows V/σ vs. redshift for the 8 tier-1 rotators, with the W15 thresholds at $V/\sigma = 1$ and $V/\sigma = 3$ marked. Panel (d) shows a heatmap of the five Wisnioski et al. (2015) disk criteria across all 8 rotators sorted by redshift.

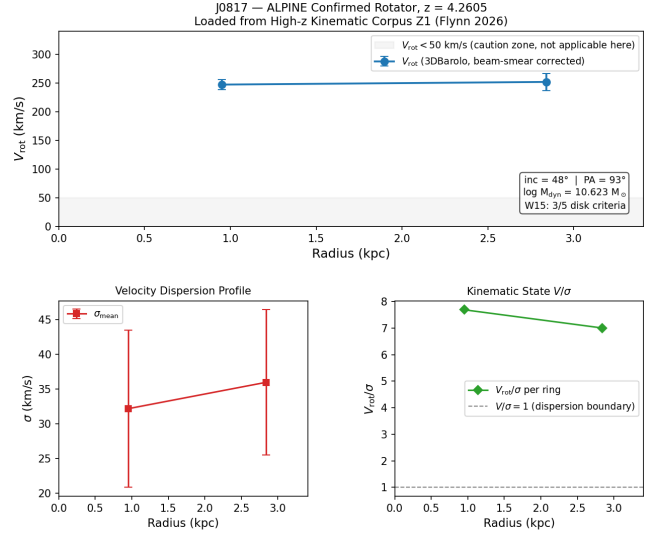


Figure 1. J0817 (ALPINE confirmed rotator, $z = 4.2605$) loaded from the Z1 corpus JSON. *Top:* V_{rot} with 3DBarolo error bars (beam-smear corrected). *Bottom left:* Velocity dispersion profile. *Bottom right:* V/σ per ring. Metadata ($\text{inc} = 48^\circ$, $\text{PA} = 93^\circ$, $\log M_{\text{dyn}} = 10.623$, W15: 3/5) extracted directly from the JSON.

Population statistics from flat CSV.

```
import csv, json
from collections import Counter
galaxies_csv = []
with open('high_z_kinematic_corpus_Z1_flat.csv') as f:
    for row in csv.DictReader(f):
        galaxies_csv.append(row)
classes = [r['class_jones2021'] for r in galaxies_csv]
redshifts = [float(r['redshift']) for r in galaxies_csv]
class_counts = Counter(classes)
n_z5 = sum(1 for z in redshifts if z > 5.0)
```

Notably, two of the three $z > 5$ rotators (DC552206, $\sigma_{\text{mean}} = 83.1 \text{ km s}^{-1}$; HZ9, $\sigma_{\text{mean}} = 50.3 \text{ km s}^{-1}$) have mean dispersions exceeding 50 km s^{-1} , consistent with the elevated turbulence expected in high- z star-forming disks (Wisnioski et al. 2015). These values are available only for tier-1 galaxies; the 6 non-ROT galaxies at $z > 5$ have no reliable σ estimate.

5.3. Example 3: Cross-Corpus Omega Kinematic Application

Figure 3 demonstrates an application of the Flynn & Cannaliato (2025) omega kinematic correction to the Z1 tier-1 rotators, connecting the high- z corpus to the $z = 0$ EPS Research corpora. This example is illustrative; the caveats in Section 7 apply in full.

Applying Equation (1) to all 8 tier-1 rotators using the `data[0]` and `data[-1]` boundary points yields

Table 3. Tier-1 confirmed rotators: outermost ring properties.

Galaxy	z	N_{rings}	r_{max} (kpc)	$V_{\text{rot,out}}$ (km s^{-1})	$e_{V_{\text{rot}}}$ (km s^{-1})	σ_{out} (km s^{-1})	V/σ	W15
J0817	4.2605	2	2.84	252.09	14.94	35.98	7.006	3/5
CG32	4.4105	2	3.50	115.04	26.96	19.14	6.010	4/5
DC396844	4.5424	2	3.75	80.42	17.66	19.84	4.053	2/5
VC5110377875	4.5506	2	3.84	102.85	19.84	60.84	1.690	3/5
DC881725	4.5778	2	3.44	62.07	12.54	48.40	1.282	3/5
DC552206	5.5016	3	5.53	172.84	27.63	65.34	2.645	3/5
HZ9	5.5413	3	2.68	176.63	25.45	4.82	36.645	2/5
DC494057	5.5446	2	3.13	80.31	12.75	44.98	1.785	2/5

NOTE— r_{max} : outermost ring radius. $V_{\text{rot,out}}$, σ_{out} : velocity and dispersion at outermost ring. Inclination uncertainty not propagated into V_{rot} errors (3DBarolo systematic; see Jones et al. 2021 Section 5.3.2). HZ9 outer-ring $\sigma = 4.82 \text{ km s}^{-1}$ is anomalously low relative to inner rings ($\sigma \sim 71\text{--}75 \text{ km s}^{-1}$); see Section 4.

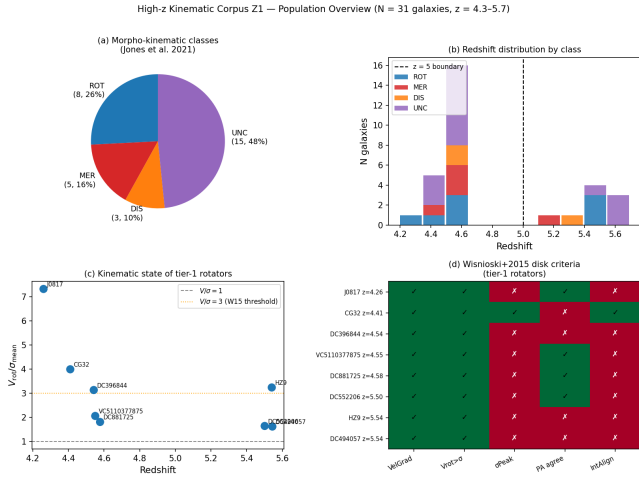


Figure 2. High-z Kinematic Corpus Z1 population overview ($N = 31$ galaxies, $z = 4.3\text{--}5.7$). (a) Morpho-kinematic class fractions from Jones et al. (2021). (b) Redshift distribution by class (stacked histogram); dashed line marks $z = 5$. (c) V/σ vs. redshift for tier-1 rotators; dotted lines at $V/\sigma = 1$ and $V/\sigma = 3$ (W15 threshold). (d) Wisnioski et al. (2015) disk criteria heatmap for all 8 rotators sorted by redshift. CG32 passes 4/5 criteria (most robustly confirmed disk); HZ9 and DC396844 pass 2/5.

the values in Table 4. All 8 values are negative (median $\omega = -13.05 \text{ rad Gyr}^{-1}$, range -33.22 to $-2.96 \text{ rad Gyr}^{-1}$), indicating falling angular velocity profiles (V/R decreasing outward). This contrasts with positive ω values at $z = 0$: SPARC mean $+7.06 \pm 3.26 \text{ rad Gyr}^{-1}$ across 84 galaxies (Flynn & Cannaliato 2025), and dwarf/irregular median $+9.94 \text{ rad Gyr}^{-1}$ across 24 ω -ready galaxies (Flynn 2026b).

Omega computation from CII boundary velocities.

```

import json, numpy as np
with open('high_z_kinematic_corpus_Z1.json') as f:
    corpus = json.load(f)
rotators = [g for g in corpus['galaxies']
             if g.get('is_rotator') and
             g.get('quality_tier') == 1]

results = []
for g in rotators:
    d = g['data']
    R1, V1 = d[0]['R_kpc'], d[0]['Vrot_kms']
    R2, V2 = d[-1]['R_kpc'], d[-1]['Vrot_kms']
    omega = (V2/R2 - V1/R1) * (R1/R2)**1.5
    results.append({'galaxy': g['galaxy'],
                  'z': g['redshift'],
                  'omega': omega})

```

The sign reversal across cosmic time is consistent with the known evolution from compact, centrally concentrated systems at high z to extended rotating disks at $z = 0$, but does not constitute a test of the ω framework in the absence of baryonic decomposition. The Z1 corpus provides the observational boundary condition for future RAMSES cosmological simulations tracing this kinematic evolution from $z = 6$ initial conditions to $z = 0$.

6. APPLICATION TO LLM-BASED INFERENCE

A secondary design goal of the corpus is to serve as a retrieval corpus for LLM-based RAG pipelines in astrophysical research. The per-galaxy ZIP archive is opti-

Table 4. Omega values for tier-1 rotators.

Galaxy	z	R_2 (kpc)	$V_{\text{rot},2}$ (km s $^{-1}$)	ω (rad Gyr $^{-1}$)
J0817	4.2605	2.84	252.09	-33.22
CG32	4.4105	3.50	115.04	-13.05
DC396844	4.5424	3.75	80.42	-14.48
VC5110377875	4.5506	3.84	102.85	-12.73
DC881725	4.5778	3.44	62.07	-13.05
DC552206	5.5016	5.53	172.84	-2.96
HZ9	5.5413	2.68	176.63	-20.14
DC494057	5.5446	3.13	80.31	-9.53

NOTE—Omega computed from Equation (1) using boundary points `data[0]` and `data[-1]`. All values negative, indicating falling V/R profiles. Median $\omega = -13.05$ rad Gyr $^{-1}$. DC552206 has a rising V_{rot} profile ($V_2 > V_1$) but negative ω because V/R decreases outward. No baryonic decomposition available; direct comparison to $z = 0$ requires caution (Section 7).

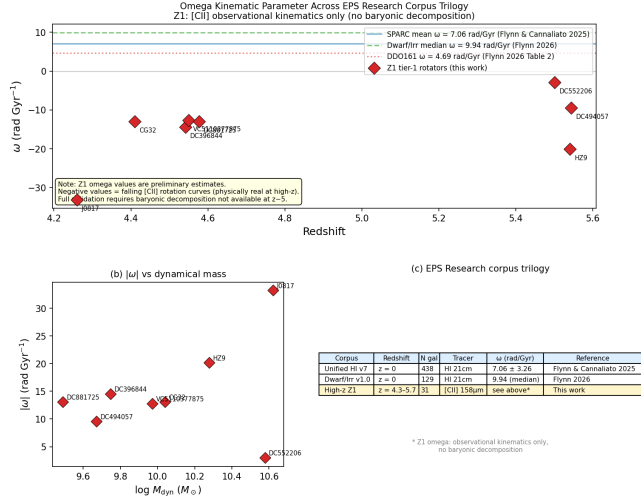


Figure 3. Cross-corpus omega application. (a) ω vs. redshift for Z1 tier-1 rotators (diamonds) with $z = 0$ reference lines: SPARC mean $+7.06$ rad Gyr $^{-1}$ (blue solid), dwarf/irregular median $+9.94$ rad Gyr $^{-1}$ (green dashed), DDO161 $+4.69$ rad Gyr $^{-1}$ (red dotted). Orange diamonds: negative ω ; all 8 rotators show falling angular velocity profiles at $z \sim 4-6$. (b) $|\omega|$ vs. $\log M_{\text{dyn}}$. (c) EPS Research corpus trilogy summary. Note: Z1 omega values are observational kinematics only; no baryonic decomposition available at $z \sim 5$ (Section 7).

mized for this use case: each file is a self-contained JSON document of $\sim 3-5$ KB, well within typical LLM context limits, containing all metadata and per-ring data needed to answer kinematic queries without external lookups.

To assess whether the JSON schema is sufficiently self-describing for automated consumption, we conducted a structured usability evaluation with four LLMs: Google Gemini Pro, Anthropic Claude, Microsoft Copilot Pro, and Gemma 4 31B Dense (self-hosted via LM Studio on Node1). Each model was presented with a single per-galaxy JSON document and asked to perform three benchmark tasks without additional documentation: (1) plot the [CII] rotation curve with error bars; (2) compute V/σ for all tier-1 rotators from the flat CSV; and (3) apply the Flynn & Cannaliato (2025) omega formula to a specified galaxy. All four models successfully generated syntactically correct Python for all three tasks on first attempt, requiring no additional prompting beyond a natural-language research question, consistent with the findings of Flynn (2026a) for the local HI corpora. These results suggest that the corpus’s explicit column definitions, unit annotations, and quality flags provide sufficient context for LLM-based code generation without external documentation.

7. KNOWN LIMITATIONS

Ten limitations should be noted by users of this corpus.

(1) *Maximum redshift is $z = 5.6773$, not $z = 6$.* The corpus designation “Z1” reflects its role as the high- z anchor of the EPS Research series, approaching but not reaching $z = 6$. The highest-redshift galaxy is DC773957 ($z = 5.6773$). True $z = 6$ spatially resolved [CII] rotation curves at astrophysically useful resolution do not yet exist. The schema is designed to accommodate future REBELS, CRISTAL, and JWST IFU samples.

(2) *Only 8/31 galaxies have per-ring rotation curve data.* The remaining 23 carry morpho-kinematic classification only.

(3) *2–3 rings per tier-1 galaxy.* Omega and dynamical mass estimates are sensitive to boundary conditions with so few radial points.

(4) *No baryonic decomposition.* V_{gas} and V_{disk} are not available at $z \sim 5$; omega values are observational kinematics, not baryonic-model-corrected values. Direct comparison to $z = 0$ omega requires future baryonic modeling.

(5) *Beam smearing.* All ALPINE data has ~ 1 arcsec beam ($\sim 6-7$ kpc at $z \sim 5$). 3DBarolo mitigates but does not eliminate beam-smearing effects.

(6) *ALPINE selection bias.* The survey targets $\text{SFR} > \text{few } M_{\odot} \text{ yr}^{-1}$, missing the true progenitor population of local dwarf irregulars ($\log M_* \sim 7.5$ at $z = 0$). Progenitor candidates identified in Example 3 are upper-mass analogs, not confirmed DDO161-class progenitors.

(7) *[C II] vs. HI tracer difference.* Direct kinematic comparison between Z1 ([C II]) and the $z = 0$ corpora (HI 21 cm) requires caution; the tracers sample different gas phases and spatial scales.

(8) *$M_{\text{dyn}} < M_*$ for CG32 and DC396844.* Dynamical mass below stellar mass is physically implausible and likely reflects inclination uncertainty compounded by the 2-ring boundary constraint. Values are reported as published in Jones et al. (2021).

(9) *HZ9 outer-ring dispersion anomaly.* The outermost ring of HZ9 has $\sigma = 4.82 \text{ km s}^{-1}$, anomalously low relative to inner rings ($\sigma \sim 71\text{--}75 \text{ km s}^{-1}$), likely a 3DBarolo fit artifact at the beam resolution limit.

(10) *DC519281 redshift uncertainty.* $e_z = 0.02$, approximately $40\times$ larger than the typical sample uncertainty, reflecting genuine spectroscopic uncertainty in this source.

8. DATA AVAILABILITY

The corpus is publicly available at Zenodo under DOI: [10.5281/zenodo.20369285](https://doi.org/10.5281/zenodo.20369285). The deposit includes the master JSON, flat CSV, JSONL, per-galaxy ZIP archive, three Jupyter notebooks with output figures, and the ingestion and validation scripts. The corpus schema, normalization, and unified structure are original work by D.C. Flynn / EPS Research and are released under CC BY 4.0. All underlying kinematic data are drawn from published, publicly available sources; users should cite both this corpus and the relevant primary survey papers listed in the references.

This corpus is the fourth in the EPS Research RAG Astrophysics Corpus Series. The companion corpora are available at: Unified HI Corpus v7.0 (Flynn 2026a), DOI: [10.5281/zenodo.19563417](https://doi.org/10.5281/zenodo.19563417); Dwarf/Irregular Corpus v1.0 (Flynn 2026b), DOI: [10.5281/zenodo.20320362](https://doi.org/10.5281/zenodo.20320362); Milky Way GC Corpus v1.3.1 (Flynn 2026c), DOI: [10.5281/zenodo.19907765](https://doi.org/10.5281/zenodo.19907765).

1 This work was conducted as independent research by
 2 EPS Research without external funding or institutional
 3 affiliation. The author thanks Jim Cannaliato for col-
 4 laboration on the omega correction framework. The
 5 ALPINE survey team is thanked for making their kine-
 6 matic catalog and data products publicly available. The
 7 ALMA Observatory is operated by ESO, AUI/NRAO,
 8 and NAOJ.

DECLARATION OF GENERATIVE AI USE

In accordance with standard practice for AI-assisted research, the author discloses the following. Four large language models were used during the creation and validation of this corpus and manuscript: Google Gemini Pro, Anthropic Claude (Sonnet and Opus), Microsoft Copilot Pro, and Gemma 4 31B Dense (self-hosted). Because the corpus is explicitly designed for LLM-based RAG pipelines, these models served as both development tools and validation instruments:

(1) *Corpus schema design and ingestion code.* LLMs assisted in drafting and debugging the Python ingestion scripts, JSON schema design, and flat CSV generation. All code was reviewed, tested, and validated by the author against primary source data.

(2) *Multi-model schema validation.* As described in Section 6, Gemini Pro, Claude, Copilot Pro, and Gemma 4 31B Dense were each tested as downstream consumers of the corpus JSON to verify that the schema is sufficiently self-describing for LLM-based scientific analysis without additional prompting.

(3) *Cross-model review.* Prior to Zenodo submission, five LLMs (Gemini Pro, Claude, Copilot Pro, Gemma 4 31B, and AstroSage-70B) were asked to review the corpus files and README for data anomalies and documentation inconsistencies. This process identified the maximum redshift attribution error (DC417567 vs. DC773957) that was corrected prior to publication.

(4) *Manuscript preparation.* Claude (Anthropic) assisted in drafting, formatting, and assembling this manuscript. All scientific content, interpretations, data provenance decisions, and editorial judgments are the sole responsibility of the author.

No generative AI output was accepted without human review. The author takes full responsibility for the content of this publication.

REFERENCES

- B ethermin, M., Fudamoto, Y., Ginolfi, M., et al. 2020, A&A, 643, A2.
<https://doi.org/10.1051/0004-6361/202037649>
- Di Teodoro, E.M., & Fraternali, F. 2015, MNRAS, 451, 3021. <https://doi.org/10.1093/mnras/stv1213>
- Faisst, A.L., Schaerer, D., Lemaux, B.C., et al. 2020, ApJS, 247, 61. <https://doi.org/10.3847/1538-4365/ab7a3c>

- Flynn, D.C., & Cannaliato, J. 2025, *Frontiers in Astronomy and Space Sciences*, 12.
<https://doi.org/10.3389/fspas.2025.1680387>
- Flynn, D.C. 2026a, *Astronomy and Computing* (submitted; preprint arXiv:2604.13489). Zenodo.
<https://doi.org/10.5281/zenodo.19563417>
- Flynn, D.C. 2026b, *Dwarf/Irregular Galaxy HI Rotation Curve Corpus v1.0*. Zenodo.
<https://doi.org/10.5281/zenodo.20320362>
- Flynn, D.C. 2026c, *Milky Way Globular Cluster Corpus v1.3.1*. Zenodo. <https://doi.org/10.5281/zenodo.19907765>
- Jones, G.C., Vergani, D., Romano, M., et al. 2021, *MNRAS*, 507, 3540. <https://doi.org/10.1093/mnras/stab2703>
- Le Fèvre, O., Béthermin, M., Faisst, A., et al. 2020, *A&A*, 643, A1. <https://doi.org/10.1051/0004-6361/201936965>
- Wisnioski, E., Förster Schreiber, N.M., Wuyts, S., et al. 2015, *ApJ*, 799, 209.
<https://doi.org/10.1088/0004-637X/799/2/209>